Advanced Powder Technology xxx (2017) xxx–xxx

Contents lists available at ScienceDirect

Advanced Powder Technology

journal homepage: www.elsevier.com/locate/apt

Original Research Paper

Thermal stability analysis of Cu-11.8 wt%Al milled samples by TEM and HT-XRD

N.N. Sanchez Pascal [a], M.F. Giordana [b,*], F. Napolitano [c], M.R. Esquivel [c,d], E. Zelaya [c]

[a] Facultad de Ingeniería – UNCo, Buenos Aires 1249, Neuquén 8300, Argentina
[b] Instituto de Física de Rosario CONICET-UNR, Ocampo 210 Bis, Rosario 2000, Argentina
[c] Centro Atómico Bariloche CNEA-CONICET, Av. Bustillo 9500, Bariloche 8400, Argentina
[d] Centro Regional Universitario Bariloche – UNCo, Quintral 1250, Bariloche 8400, Argentina

ARTICLE INFO

Article history:
Received 3 April 2017
Received in revised form 21 June 2017
Accepted 15 July 2017
Available online xxxx

Keywords:
Powder metallurgy
Shape memory alloys
Phase stability
HT-XRD
TEM

ABSTRACT

In this work, the thermal stability of two samples of Cu-11.8 wt%Al obtained by different milling processes is analyzed. Several TEM techniques were used and HT-XRD experiments performed to determine the crystal structure and the morphological microstructure of the samples obtained during different heat treatments. The heat treatments were: quenching from 850 °C to room temperature and two consecutive calorimetric runs at 5 °C/min. After the quenching,α_2 is the major phase observed, reaching 95 mass%. The remaining 5 mass% consisted of martensitic phases: one sample had γ', a hexagonal structure, and the other β_1', a rhombohedral structure. During the first calorimetric run, the sample containing the γ' phase exhibited a calorimetric event and the sample containing the β_1' phase did not. The calorimetric event is attributed to the austenitic transformation $\gamma' \rightarrow \beta_1$. The lack of calorimetric event in the sample containing the β_1' is associated with the inhibition of the transformation $\beta_1' \rightarrow \beta_1$ because of the precipitation of the γ_2 phase. Finally, the absence of a calorimetric event in the second run with the first sample is associated with the retransformation to β_1' instead to γ' phase during cooling of the first calorimetric run. These studies determined that the first sample is a better candidate than the second sample to produce a shape memory alloy after thermo-mechanical treatments of the milled powders.

1. Introduction

Shape memory alloys are smart materials that change their shape due to a diffusionless martensitic transformation between two phases at a given temperature. Among all Cu-based shape memory alloys, the ones containing Al are the most interesting due to their high transformation temperature (M_s), which is over 200 °C [1]. The martensitic transformation is reversible and takes place between solid state phases. The high-temperature phase is called austenite and the low-temperature phase martensite [2,3]. In Cu-Al alloys, the transformation occurs between the high-temperature β phase and the low-temperature β'_1 or γ' phases [4,5]. In these alloys, both the structure of the martensite phase and the temperature of the martensitic transition depend on the Al content of the sample. In the Cu-Al system, the martensitic transformation could also be hindered by either α or γ_2 phase precipitation [6–8]. It is important to briefly describe the conventional Cu-Al phase diagram in order to understand the role of the temperature for different Al concentrations in these alloys. A selected section of this binary phase diagram is shown in Fig. 1 [7]. At the highest temperature analyzed, 550 °C, the β phase has a eutectoid at 11.8 wt%Al. This phase has a disordered bcc-based structure [9,10]. For compositions near 11.8 wt%Al and temperatures less than the eutectoid, the β phase shows an order transition to a first order neighbor. The resultant phase, β_1, is ordered [9]. This phase can transform martensitically to the γ' phase when the Al content is larger than 13 wt%Al. The γ' phase has a hexagonal structure that can be also described as an AB stacking sequence [9]. The β_1 phase transforms to the β'_1 for Al contents lower than 13 wt%Al. This phase has a rhombohedral structure that can also be described as a monoclinic structure with an ABCBCACAB stacking sequence [11,12]. It is relevant to mention that the precipitation of the γ_2 phase at 200 °C can occur even from martensites with a 12 wt%Al content [6]. The γ_2 phase has a cubic structure with 52 atoms and 2 structural vacancies [13]. The decomposition of β might occur to both γ_2 and α phases [7,14]. The α phase has a fcc structure that can also be described as a solid solution of aluminum in

* Corresponding author.
E-mail address: giordana@ifir-conicet.gov.ar (M.F. Giordana).

http://dx.doi.org/10.1016/j.apt.2017.07.012

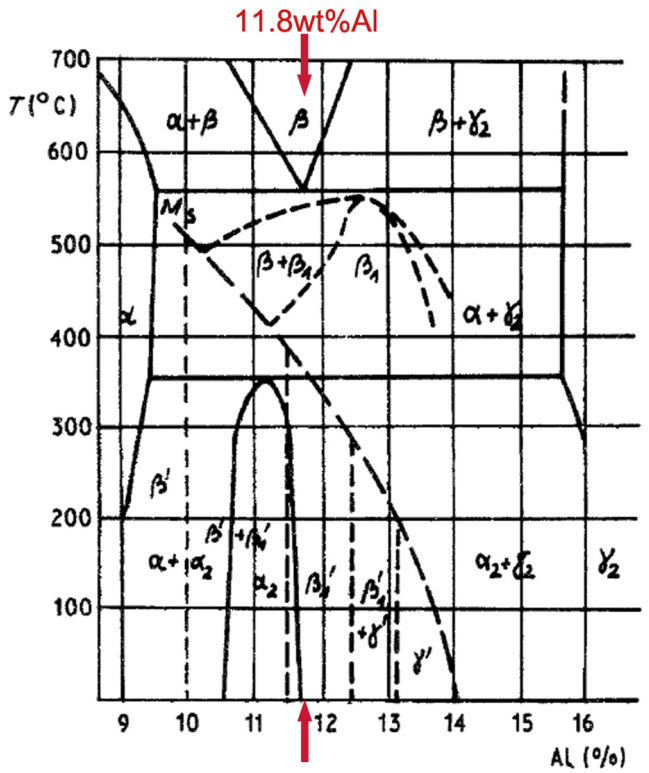

Fig. 1. A selected section of the Cu-Al alloy binary phase diagram (continuous lines). The M_s temperatures and stable regions for the different martensitic phases are shown. Red arrows indicate the composition used in this work [9]. (For interpretation of the references to colour in this figure legend, the reader is referred to the web version of this article.)

copper [1,15]. The α phase can also transform into the α_2-compact tetragonal phase at temperatures less than 340 °C [7,11].

It has been reported that novel synthesis methods for Cu-Al based intermetallics produce a decrement in the grain size that increases the average value of fracture stress in these materials [16]. These methods involve the sintering of micrometric powders with irregular particle boundaries. Reactive milling is used to control particle size and to obtain irregular particles boundaries, which favor powder cohesion [17–19]. Intermetallics in Cu based systems are produced by different types of milling [20–22]. However, the intermetallics obtained at the completion stage of the milling do not match the thermodynamic equilibria of the conventional phase diagram. This behavior has been previously reported for this system and others [21–24]. Moreover, Cu-11.8 wt%Al has a mixture of α and γ_2 phases after the final stage of milling [22]. The amount of each phase depends on the type of milling. All powder sintering techniques of the powders involve thermomechanical treatments [17–19]. For this reason, it is important to know the thermal stability of powders to be processed. The novelties presented in this work involve the synthesis and heat treatment of powder samples obtained by two different milling processes. These processes lead to different powder characteristics which, in turn, due to the differences in the energy accumulated affects the formation of the desired martensite. The austenitic transformation $\gamma' \rightarrow \beta_1$ or $\beta_1' \rightarrow \beta_1$ was fully characterized in bulk materials. However, the characteristic of this transformation or inhibition by the precipitation of γ_2 phase was never studied so deeply in powders. Moreover, most of the information available about powder process characterized the powder already compacted [16,17], without a careful study of the modification of the powder in each step of the compact process.

Thus, the aim of this work was to examine the phase stability of two powder samples with the same nominal composition obtained by different milling processes [22]. The results should show which milling process yields the best powder that can be sintered into a high quality shape memory alloy.

2. Materials and methods

2.1. Sample treatment

The thermal stability of the phases present in the samples was studied after and/or during three consecutive heat treatments. The details of each of the treatments are discussed in following sections and shown schematically in Fig. 2. In order to clarify the following text, the samples were renamed after each heat treatment.

2.2. Synthesis and characterization of samples P50 and H100

The starting samples were Cu-Al mixtures with a nominal composition of Cu-11.8 wt%Al obtained by mixing elemental Cu (99.999% purity) and Al (99.5% purity) powders. Mixtures were milled by two different milling processes. The first one was carried out for 50 h in a Fritsch Pulverissette 6 planetary-motion mill with conditions selected to fullfill medium-energy milling, that sample is labelled P50. The second sample was prepared in a Australian Instrument Uniball Mill II horizontal mill with conditions selected to reach low-energy milling for 100 h. Sample obtained is denominated H100. Synthesis details for samples P50 and H100 are published elsewhere [22]. It is worth mentioning that the milling conditions used for samples P50 and H100 were selected considering milling stages. Since composition in both cases do not change after reaching completion stage, the milling times in each case were selected to assure that both samples reached this stage [22,23]. It means that P50 reached final stage at milling times < 50 h and H100 reached this stage at 100 h. The structure and microstructure of these sample were analized by transmission electron microscopy (TEM) and X-ray diffraction (XRD). The TEM characterization was performed using both a FEI TECNAI F20 G2 field emission and a FEI CM200 UT microscopes operated at 200 keV. The phase studies were carried out at room temperature by XRD on a PANalytical Empyrean diffractometer with Cu Kα radiation. High statistic XRD profiles were analyzed with the Rietveld method using the Fullprof software [25,26].

2.3. Synthesis and characterization of samples QP50 and QH100

Samples P50 and H100 were heat treated by sealing them in quartz capsules under an Ar atmosphere and annealing in an ad-hoc designed laboratory oven. The heat treatment consists of annealing at 850 °C for 48 h followed by water quenching. From now on, this annealing and quenched is called the first heat treatment. Samples heated and water-quenched are labeled as QP50 and QH100, respectively. TEM and XRD analysis of samples QP50 and QP100 were performed in the same equipment as for samples P50 and P100.

2.4. Synthesis and characterization of samples QRP50 and QRH100

Thermal stability of the annealed and water-quenched powders (samples QP50 and QH100) was studied by differential scanning calorimetry (DSC 2910, TA Instruments). Measurements were taken between room temperature and 500 °C in a purified Ar (99.999%) atmosphere at a heating rate of 5 °C min^{-1}. The phase stability of samples QP50 and QH100 was also studied by in-situ high-temperature XRD using an Anton Paar HTK 1200 N chamber

Please cite this article in press as: N.N. Sanchez Pascal et al., Thermal stability analysis of Cu-11.8 wt%Al milled samples by TEM and HT-XRD, Advanced Powder Technology (2017), http://dx.doi.org/10.1016/j.apt.2017.07.012

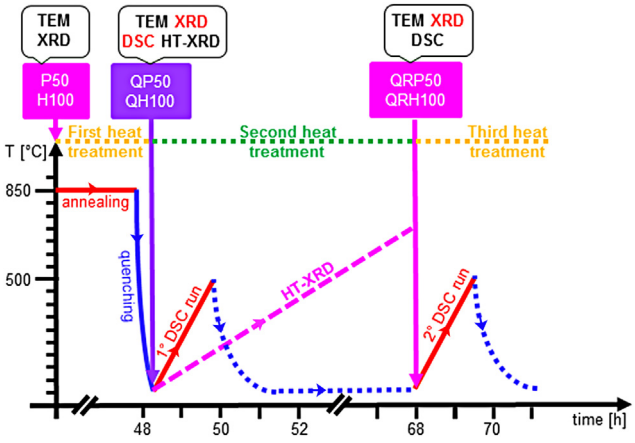

Fig. 2. Schematic representation of the heat treatments given to each sample.

with an automatic high-Z correction connected to a PANalytical Empyrean diffractometer with a PixCel 3D detector. Isothermal measurements at selected temperatures were performed with a heating program from room temperature to 700 °C using a 10 °C min^{-1} heating ramp under a He (purity 99,999%) flow of 100 ml.min^{-1}. During heating, different temperatures were selected to obtain isothermal profiles (25 °C, 200 °C, 260 °C, 280 °C, 350 °C, 450 °C, 500 °C, 550 °C, 600 °C, 650 °C, 700 °C). The time spent during each measurement for the different temperatures was one hour. From now on, the heating of the samples during the first run of DSC measurements is called the second heat treatment. After the DSC run or HT-XRD, the QP50 and QH100 samples were renamed QRP50 and QRH100, respectively. Structure and microstructure of these samples were analized by TEM and XRD in the same equipment described in Section 2.2.

2.5. Final heat treatment of samples QRP50 and QRH100

Finally, the thermal stability of samples QRP50 and QRPH100 was studied by DSC in the DSC 2910, TA Instruments. This third heat treatment was performed under the same conditions as samples QP50 and QH100, described in the previous section.

3. Results and discussion

3.1. Microstructure changes after the first heat treatment

Fig. 3 shows the variation in microstructure of sample H100 due to the application of the first heat treatment (annealing at 850 °C and quenching). Here, there is a clear microstructural change in the sample before (H100) and after (QH100) the first heat treatment. There is an observed increment in the grain size and a change of shape in the inner microstructure of some grains as clearly observed by comparing dark field images shown in Fig. 3a–d. The same characteristic and changes in microstructure are observed in samples P50 and QP50 (data not shown). The dark field images of the QH100 sample show some grains with a flat contrast and the others with bands. The bands turn on and off for different selected diffraction spots. Microstructures similar to those shown in Fig. 3c or Fig. 4a were previously reported in martensites structures with twins [27,28].

Other TEM techniques corroborate the presence of martensite structures in the contrasting bands within grains and the presence of α_2 structure in the grains having a flat contrast. As an example, Fig. 4b shows the microdiffraction of a grain with contrasting

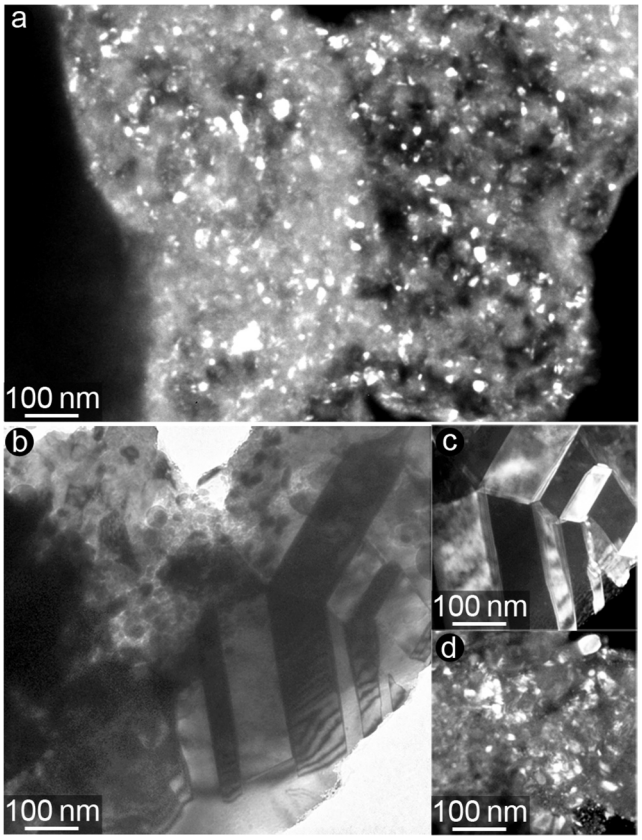

Fig. 3. (a) TEM dark field image of sample H100. (b) A bright field image of sample QH100. (c) and (d) Dark field images showing in detail the different microstructures found in the particle shown in image (b).

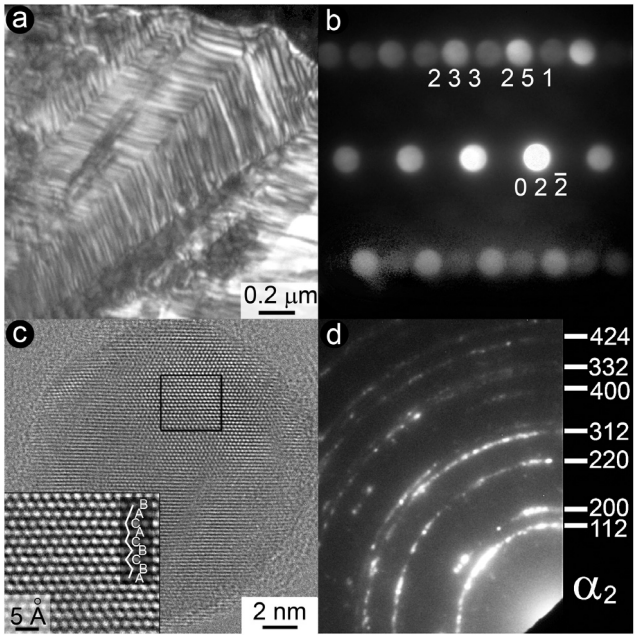

Fig. 4. (a) A TEM dark field image of sample QP50. (b) Microdiffraction pattern indexed as [3 −1 −1]γ′ zone axis of a band contrast grain in image (a). (c) HRTEM image of sample QH100. The inset presents a magnified micrograph of the rectangular area showing an ABCBCACAB stacking sequence. (d) Selected area diffraction of the grains with flat contrast from sample QP50.

Please cite this article in press as: N.N. Sanchez Pascal et al., Thermal stability analysis of Cu-11.8 wt%Al milled samples by TEM and HT-XRD, Advanced Powder Technology (2017), http://dx.doi.org/10.1016/j.apt.2017.07.012

bands in sample QP50. This pattern can be indexed as γ′ martensite. Fig. 4c shows the HRTEM image of sample QH100. The image also displays a stacking sequence that can be associated with β_1'. Fig. 4d shows the selected area diffraction of grains with flat contrast. All the ring diffraction patterns are indexed as the α_2 phase. Although both samples, QH100 and QP50, show the same type of diffraction pattern of plain contrast grains, the martensite structure in sample QP50 is consistent with the presence of γ′, while the martensite structure in sample QH100 is associated with the presence of β_1'.

The mean diameter of the grains with flat contrast is two times larger than the grains before the quenching. However, the grains that exhibit a martensite microstructure seem to grow one order of magnitude as shown in Table 1. This behavior can be attributed to an abrupt change of microstructure occurring when either the β or β_1 phase transforms martensitically during the quenching process. The difference between phase transformations could explain the differences in the grain growth. Both α and γ_2 phases nucleate and growth inside the β or β_1 phase while the martensites transform the whole microstructure of the grain at the same time.

3.2. Structure changes after the first heat treatment

Diffractograms of samples P50 and H100 are shown with continuous blue lines in Fig. 5a and b, respectively. In both cases, α and γ_2 phases were indexed. No other phase was observed within the detection limit of this technique. After the first heat treatment, different profiles were presented in each sample, since new peaks appear. Diffractograms of samples QP50 and QH100 are shown in red shading in Fig. 5a and b, respectively. The peaks indexed as phases α_2 and γ′ in sample QP50 while phases α_2 and β_1' were indexed in sample QH100. These results are consistent with TEM analysis of the quenched samples, since both types of phases grow in each sample.

The Rietveld refinement of the QP50 and QH100 samples X-ray diffraction patterns show that α_2 is the major phase. Although the martensite structures in both samples are different, the mass content of these phases is less than 7%. Results are summarized in Tables 2 and 3. The lattice parameters of the martensites and the α_2 phases, also obtained from the Rietveld analysis, match previous reported values [7,9,11,12]. It should be also pointed out that in Fig. 5 the α_2 peaks in the diffraction patterns of samples QP50 and QH100 are narrower than peaks corresponding to α and γ_2 phases of samples P50 and H100. The profile changes can be mostly attributed to two different processes. Firstly there is the relaxation of retained strains during the milling process. Secondly there is grain growth. Also, peaks of α_2 phase seem narrower than those peaks associated with the martensitic phases γ′ and β_1' of samples QP50 and QH100. α_2 phase grains growth to twice the original size, as is shown in Table 1. Although β_1' and γ′ grain sizes grow one order of magnitude, as is shown in the same table, this grain growth is not apparent in the diffractogram shown in Fig. 5. This is due to two reasons: the β_1' and γ′ mass percent is low as shown in Tables 2 and 3; and the structure contains a large number of variants as displayed in Fig. 3. Therefore, the peaks from this structure are not unique. Rather, they appear as a distribution.

Table 1
Grains size ranges before and after the first heat treatment.

Sample name	Range of grain diameters [nm]	Sample name	Range of grain diameters [nm]	
			Flat contrast	Band contrast
P50	3–32	QP50	9–64	215–1038
H100	1–25	QH100	8–67	24–585

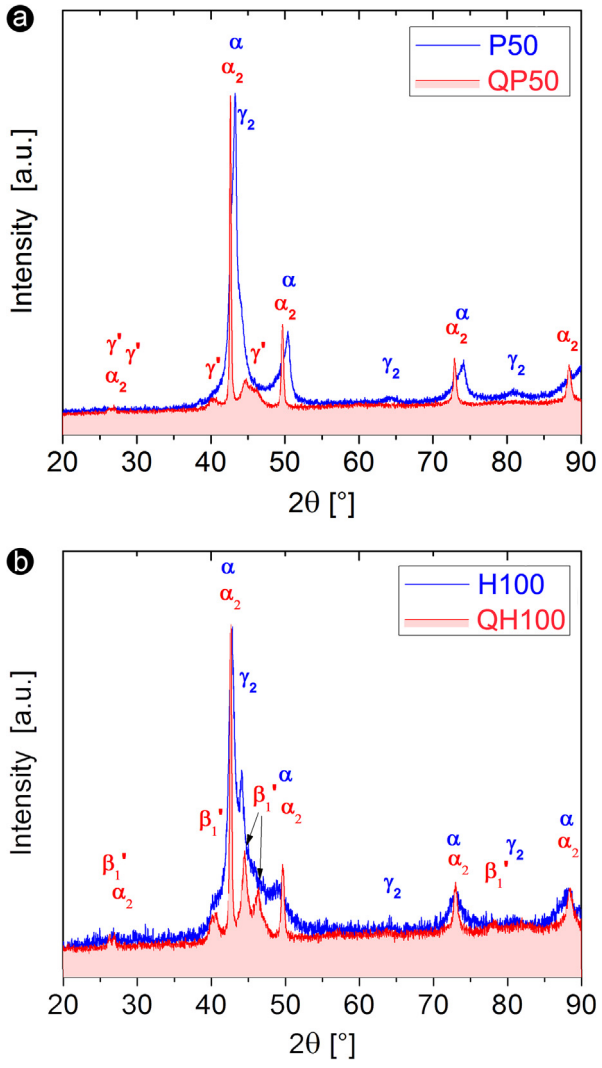

Fig. 5. X-ray diffractograms of samples (a) P50 and QP50, (b) H100 and QH100.

The difference in the type of martensite between samples QP50 and QH100 can be attributed to different amounts of α and γ_2 phase in the sample QP50 [22]. Different types of milling processes lead to different amount of intermetallics in the final stage of milling [22]. As a result, the type of martensites obtained after the quenching process are different.

3.3. Evolution of phases during second heat treatment

3.3.1. Calorimetry experiment

Fig. 6 a and b show the corresponding calorimetric evolution of samples QP50 and QH100 during the second heat treatment. As summarized in Tables 2 and 3, the only difference between these samples is the structure of the martensite. In each sample, the amount of martensite is less than the 7 mass%. The α_2 phase is the majority constituent in each sample. This structure is the stable one according to the equilibrium phase diagram shown in Fig. 1. During the first run, sample QP50 shows at least two global exothermal events between 190 °C and 480 °C while sample QH100 shows no calorimetric event. The exothermal events in QP50 are associated with one of the following processes:

(1). the decomposition of α_2 to α + γ_2
(2). the martensitic transformation of γ′ to β_1.

Please cite this article in press as: N.N. Sanchez Pascal et al., Thermal stability analysis of Cu-11.8 wt%Al milled samples by TEM and HT-XRD, Advanced Powder Technology (2017), http://dx.doi.org/10.1016/j.apt.2017.07.012

Table 2
Phase characterization of sample QP50 using the Rietveld method.

Sample QP50								
Phases	Cell parameters						Mass fraction (%)	χ^2
	Lattice parameters (nm)			Angles (°)				
	a	*b*	*c*	α	β	γ		
α_2 (*I*4/*mmm*)	0.3668(7)	0.3668(7)	0.7346(5)	90	90	90	95 ± 3	2
γ' (*Pmmn*)	0.5182(0)	0.4178(6)	0.4499(5)	90	90	90	5 ± 3	

Table 3
Phase characterization of sample QH100 using the Rietveld method.

Sample QH100								
Phases	Cell parameters						Mass fraction (%)	χ^2
	Lattice parameters (nm)			Angles (°)				
	a	*b*	*c*	α	β	γ		
α_2 (*I*4/*mmm*)	0.3668(7)	0.3668(7)	0.7346(5)	90	90	90	92 ± 3	2
β_1' (*P*2/*m*)	0.4473(7)	0.5152(1)	1.3743(9)	90	77.5303	90	7 ± 3	

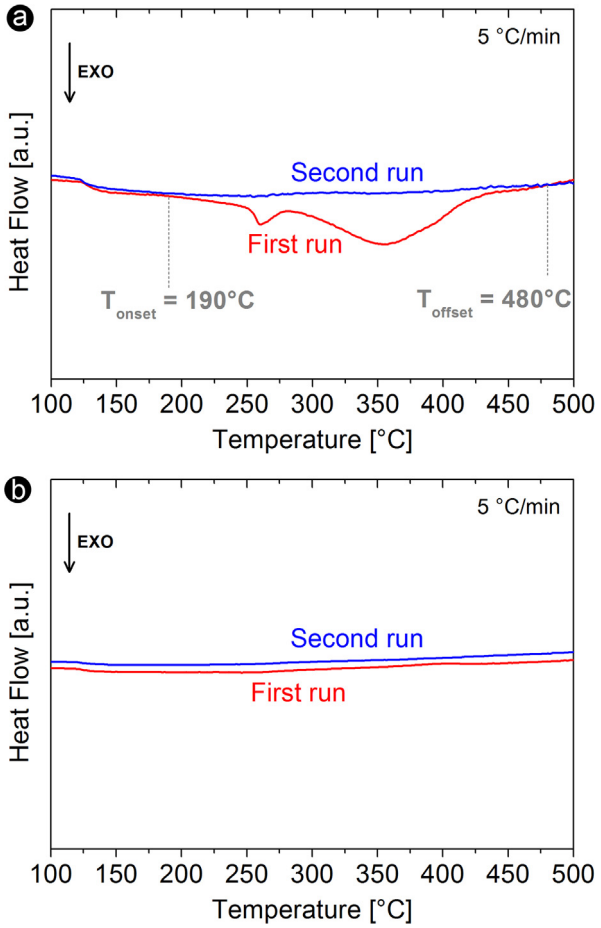

Fig. 6. DSC curves obtained at a heating rate of 5 °C min^{-1} for samples (a) QP50 and (b) QH100.

Since both samples have, within experimental error, a similar mass content of the α_2 phase, the first hypothesis does not explain the absence of a calorimetric event in sample QH100, as shown in Fig. 5b. The second hypothesis ($\gamma' \rightarrow \beta_1$) leads to the following questions concerning the absence of a calorimetric event in sample QH100.

If the martensitic transformation $\gamma' \rightarrow \beta_1$ occurs in sample QP50, it seems odd that the martensitic transformation $\beta_1' \rightarrow \beta_1$ does not involve any calorimetric event in QH100. That being the case, should it be possible that either the microstructure inhibits a calorimetric event or the transformation $\beta_1' \rightarrow \beta_1$ does not occur in sample QH100? To resolve which process occurs, in-situ HT-XRD measurements were performed, as explained in Section 3.3.2.

As observed in Fig. 6 a and b, a second calorimetric run was done. The experimental runs for each sample show identical characteristics and no thermal event is observed in either case. The lack of a heat event in the samples is discussed in Sections 3.4.1 and 3.4.2.

3.3.2. In situ HT-XRD experiments

Fig. 7a shows three different diffractograms of sample QP50 at the temperatures of 25 °C, 350 °C and 650 °C (these are particular cases selected from the 11 measured temperatures). The diffraction patterns were taken from each sample using an isothermal program in the same run. These three diffractograms show evidence of particular phases. Phases α_2 and γ' were indexed at 25 °C. Peaks of α and β_1 appeared at 350 °C and phases α and β were found at 650 °C. Two general features are associated with the sample microstructure as the temperature increases. One is the phase evolution described by the formation of new phases. The other is the general microstructure development, which shows a refinement of the peaks that correlate with grain growth and a release of residual strain. As observed, peaks are narrower as temperature increases. This behavior is associated with the relaxation of internal stresses and grain growth. Fig. 7b shows the evolution of phases at each temperature. Here, the relative intensity of the highest peak of each phase is plotted against temperature. There is a diffractogram for each temperature and all diffractograms show the coexistence of only two phases. The relative intensity indicates the increment and decrement of phase amounts. Dissolution and nucleation are also associated with these relative sample amounts. As observed in Fig. 7b, the $\gamma' \rightarrow \beta_1$ transformation takes place between 200 °C and 450 °C. This temperature range matches, within the experimental error, the exothermal event of sample QP50, shown in Fig. 6.a. Similar events measured by calorimetry are reported in a sample Cu-12.4 wt%Al [7,14]. In these references, the authors associated the calorimetric event near 400 °C with the $\gamma' \rightarrow \beta_1$ transformation. They also report a uniform martensitic grain size distribution because their alloy was prepared by induction melting. To the contrary, the grain size distribution of the

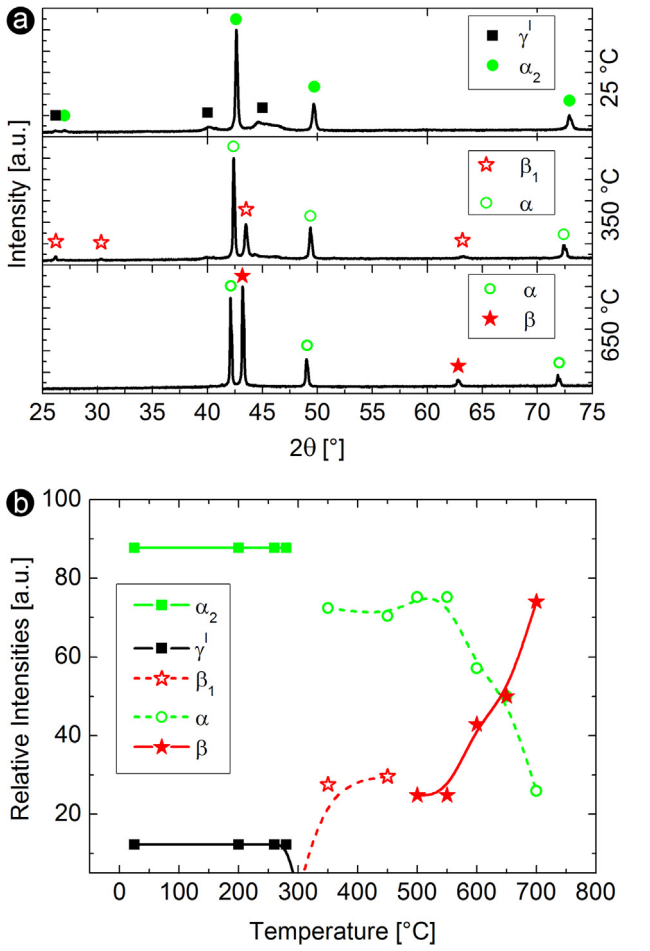

Fig. 7. (a) X-ray diffractograms of sample QP50 obtained at 25 °C, 350 °C and 650 °C. (b) Relative intensities of the highest X-ray peak of each phase of sample QP50 as a function of temperature.

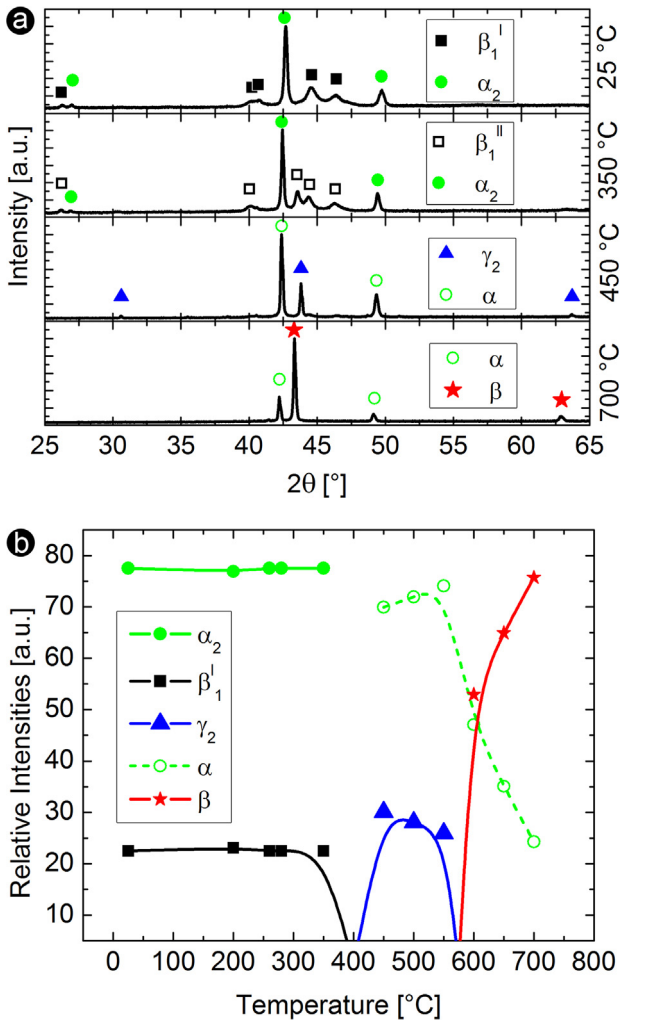

Fig. 8. (a) X-ray diffractograms of sample QH100 obtained at 25 °C, 350 °C, 450 °C and 700 °C. (b) Relative intensities of the highest X-ray peak of each phase of sample QH100 as a function of temperature.

martensite (γ' phase) in sample QP50 varies almost one order of magnitude (between 215 and 1038 nm) as shown in Table 1. Previous work with Cu-Al based alloys report a shift in the transformation temperature $\beta_1 \rightarrow \gamma'$ when the grain size is smaller than 100 μm. This temperature shift is larger for grain sizes less than 20 μm [29]. This can explain the 200 °C difference in the calorimetric event found in this work and that reported in [7,14].

Fig.8a shows four different diffractograms from sample QH100 taken at 25 °C, 350 °C, 450 °C, and 700 °C. All diffractograms were acquired during the same run in the fashion described previously. It is notable that the peaks are narrower as temperature increases, indicating both internal stress relaxation and grain growth. Nucleation, disappearance or ordering of a phase occurred at each of the four temperatures. At 350 °C, β_1' transforms to β_1'' in a first order neighbor change. At 450 °C, both β_1'' and α_2 disappear while both α and γ_2 nucleate and grow. Finally, at 700 °C, γ_2 dissolves and the β phase nucleates leading to the appearance of α. Fig. 8b shows a summary of dissolution and nucleation of each phase for the eleven isothermal measurements in the HT-XRD run. In this Figure, it is shown the relative intensity of the highest peak of each phase as a function of the isothermal measurement. Figs. 7b and 8b are similar up to 350 °C.

In Fig. 8b, nucleation of the β phase is observed at higher temperature as a consequence of the nucleation of the γ_2 phase. Then, the transformation $\beta_1' \rightarrow \beta_1$ in sample QH100 is inhibited by the precipitation of the γ_2 phase. It is worth noting that the calorimetric event in Fig. 6a of sample QP50 is associated to the transformation $\gamma' \rightarrow \beta_1$. Since the transformation of $\beta_1' \rightarrow \beta_1$ is inhibited, no appreciable calorimetric event was expected for the QH100 sample as observed in Fig. 6b. The inhibition of martensitic transformation by the γ_2 precipitation was reported for several Cu based shape memory alloys [6,30]. Again, it is worth mentioning that all these studies report that the martensitic transformation is hindered by γ_2 precipitation.

3.4. Resulting phases after the second heat treatment

3.4.1. Microstructural results

The lack of thermal events during the second heat treatment of sample QRH100 is elucidated in the previous section. However, it is not clear why there is an absence of a thermal event in the second run of sample QRP50. A possible explanation could be attributed to a change in the microstructure of the sample. Either an increment in the amount of dislocations or the precipitation of other phases can hinder or even inhibit the retransformation of the sample [6,31]. For this reason, a detailed analysis of samples QRH100 and QRP50 was carried out by TEM. Fig. 9 show a bright field image of sample QRP50. Two types of grains were observed. One type has a characteristic martensite contrast and the other, indicated with arrows, shows a plain contrast. No evidence of new precipitates

Please cite this article in press as: N.N. Sanchez Pascal et al., Thermal stability analysis of Cu-11.8 wt%Al milled samples by TEM and HT-XRD, Advanced Powder Technology (2017), http://dx.doi.org/10.1016/j.apt.2017.07.012

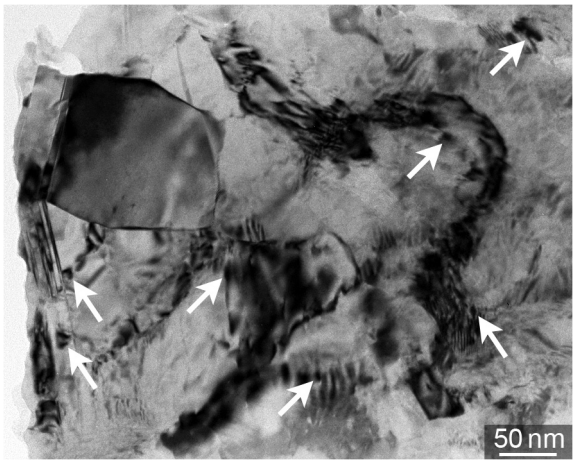

Fig. 9. Bright field TEM image of sample QRP50.

or dislocations was observed. The microstructure of sample QP50 before and after the second heat treatment was similar, as deduced by comparing Fig. 9 to Fig. 3.

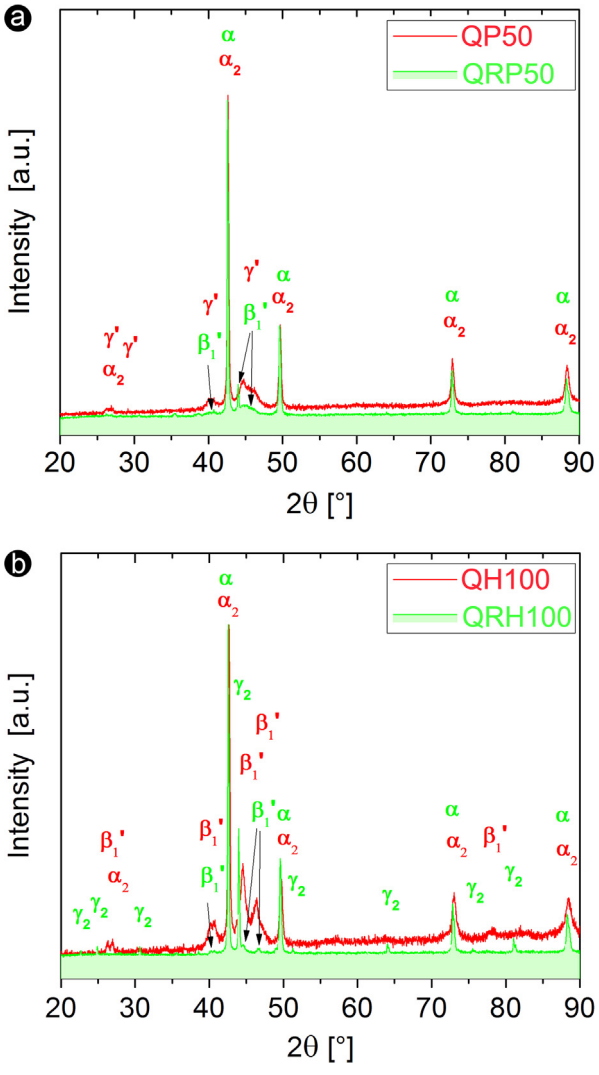

Fig. 10. X-ray diffractograms after the first and second heat treatments of samples (a) P50 and (b) H100.

3.4.2. Structural results

No clear evidence in the change of microstructure can explain the lack of a calorimetric event in sample QRP50. For this reason, room temperature XRD was performed on both QRP50 and QRH100 samples. A comparison between XRD diffractograms acquired from samples after the first and second heat treatments is shown in Fig. 10. Fig. 10a indicates that after the first calorimetric run, the γ' phase disappears and the β_1' phase is the only martensite remaining in sample QRP50. This result implies that during the cooling of QP50 sample, after the second heat treatment, the martensitic transformation $\beta_1 \rightarrow \beta_1'$ occurred instead of the $\beta_1 \rightarrow \gamma'$ martensitic transformation. Therefore, sample QRP50 shows the same type of martensite as sample QH100. The thermal event does not occur in the second calorimetric run of sample QRP50 because the precipitation of γ_2 inhibits the $\beta_1' \rightarrow \beta_1$ transformation. The retransformation of β_1 phase to other martensite structure was previously reported in other Cu based shape memory alloys [32]. This kind of behavior is activated by temperature in samples with large numbers of defects i.e. dislocations or a large grain boundary area. The grain boundary area increases as the grain size decrease. Therefore, a possible explanation of the retransformation to the type of other martensite is that the number of variants inside each martensite grain is high enough to inhibit the transformation to γ' phase.

Fig. 10b shows the evolution of the structure of sample QH100 before and after the second heat treatment. It is worth mentioning that the peaks associated with the β_1' are less intense after the second heat treatment. New peaks, associated with the γ_2 phase, are detected in the same diffractogram. This implies that the γ_2 phase is retained during the cooling of sample QH100 after the first calorimetric run. Thus, the martensitic transformation is completely inhibited by the nucleation and growth of the γ_2 phase.

4. Conclusions

The phase stability during different heat treatment was studied for two Cu-11.8%wtAl samples obtained by different milling methods. Both samples show the same microstructure after quenching: small α_2 phase grains (~35 nm) and large martensitic grains (~500 nm) containing a large number of variants. However, 5 wt % of the martensite in each sample had a different structure: γ' in sample QP50 and β'_1 in sample QH100. This difference is associated with the stability of different phases in the final stage of each milling process. While sample QP50 shows a calorimetric event, this feature is not observed in sample QH100. This calorimetric event observed in QP50 is associated with the $\gamma' \rightarrow \beta_1$ austenitic transformation, which was observed through HT-XRD experiments. In addition, the inhibition of the $\beta_1' \rightarrow \beta_1$ transformation by the precipitation of γ_2 phase was detected with HT-XRD analysis in sample QH100. Finally, the absence of a calorimetric event in the second run of sample QRP50 was studied by TEM and XRD. It is associated with the retransformation to the β_1' instead of the γ' phase during cooling in the first calorimetric run.

The possible presence of an austenitic transformation indicates that sample P50 is a better candidate than sample H100 for producing a shape memory alloy after thermo-mechanical treatments of the milled powders.

Acknowledgments

The authors express their thanks to the Consejo Nacional de Investigaciones Científicas y Técnicas (CONICET), to the Agencia Nacional de Promoción Científica y Tecnológica (ANPCyT: PICT-2015-1641), to the Comisión Nacional de Energía Atómica (CNEA) and to the Universidad Nacional del Comahue (UNCo: PI-B202-

2017) for supporting this work. Dr. Marcos Sade is thanked for fruitful discussions and we are grateful to Adriano Geraci for his assistance in using the TEM.

References

[1] M.A. Dvorack, N. Kuwano, S. Polat, Haydn Chen, C.M. Wayman, Decomposition of a β_1-phase Cu-Al-Ni alloy at elevated temperature, Scri. Metall. 17 (1983) 1333–1336.
[2] M. Ahlers, Martensite and equilibrium phases in Cu-Zn and Cu-Zn-Al alloys, Prog. Mater. Sci. 30 (1986) 135–186.
[3] K. Otsuka, H. Sakamoto, K. Shimizu, Successive stress-induced martensitic transformations and associated transformation pseudoelasticity in Cu-Al-Ni alloys, Acta Metall. 27 (1979) 585–601.
[4] B. Graczykowski, P. Biskupski, B. Mroz, S. Mielcarek, M.L. No, J. San Juan, Elastic properties of Cu–Al–Ni shape memory alloys studied by dynamic mechanical analysis, Smart Mater. Struct. 19 (2010) 15010–15018.
[5] R.A.G. Silva, E.S. Machado, A.T. Adorno, A.G. Magdalena, T.M. Carvalho, Completeness of α-phase decomposition reaction in Cu–Al–Ag alloys, J. Therm. Anal. Calorim. 927–931 (2012).
[6] V.E.A. Araujo, R. Gastien, E. Zelaya, J.I. Beiroa, I. Corro, M. Sade, F.C. Lovey, Effects on the martensitic transformations and the microstructure of CuAlNi single crystals after ageing at 473 K, J. Alloys Compd. 641 (2015) 155–161.
[7] J. Kwarciak, Z. Bojarski, H. Morawiec, Phase transformation in rnartensite of Cu-12.4% Al, J. Mater. Sci. 21 (1986) 788–792.
[8] H. Cheniti, M. Bouabdallah, E. Patoor, High temperature decomposition of the β_1 phase in a Cu–Al–Ni shape memory alloy, J. Alloys Compd. 476 (2009) 420–424.
[9] P.R. Swann, H. Warlimont, The electron-metallography and crystallography of copper–aluminum martensites, Acta Metall. 11 (6) (1963) 511–527.
[10] T.B. Massalski, The Al_Cu (aluminum–copper) system, J. Phase Equilib. 1 (1) (1980) 27–33.
[11] G. Roulin, P. Duval, Initial stages of ordering obtained by tempering of disorder martensitic phase of Cu–Al alloys, Scr. Mater. 37 (1997) 45–51.
[12] Z. Nishiyama, J. Kakinoki, S. Kajiwara, Stacking fault in the martensite of Cu–Al alloy, J. Phys. Soc. Jpn. 20 (7) (1965) 1192–1211.
[13] S. Westman, Refinement of the gamma-Cu_9Al_4 structure, Acta Chem. Scand. 19 (1965) 1411–1419.
[14] J. Kwarciak, Phase transformations in Cu-AI and Cu-Zn-Al alloys, J. Therm. Analysis 31 (1986) 559–566.
[15] T.B. Massalski, J.L. Murray, L.H. Bennett, H. Baker, Binary Alloy Phase Diagrams, vols. 1 and 2, American Society for Metals, Metals Park, OH, 1986.
[16] S.K. Vajpai, R.K. Dube, S. Sangal, Application of rapid solidification powder metallurgy processing to prepare Cu–Al–Ni high temperature shape memory alloy strips with high strength and high ductility, Mater. Sci. Eng. A 570 (2013) 32–42.
[17] S. Pourkhorshidi, N. Parvin, M.S. Kenevisi, M. Naeimi, H. Ebrahimnia Khaniki, A study on the microstructure and properties of Cu-based shape memory alloy produced by hot extrusion of mechanically alloyed powders, Mater. Sci. Eng. A 556 (2012) 658–663.
[18] A. Ibarra, P.P. Rodríguez, V. Recarte, J.I. Pérez-Landazábal, M.L. Nó, J. San Juan, Internal friction behaviour during martensitic transformation in shape memory alloys processed by powder metallurgy, Mater. Sci. Eng A 370 (2004) 492–496.
[19] S.M. Tang, C.Y. Chung, W.G. Liu, Preparation of Cu-Al-Ni-based shape memory alloys by mechanical alloying and powder metallurgy method, J. Mater. Processing Technol. 63 (1997) 307–312.
[20] S.K. Pabi, B.S. Murty, Mechanism of mechanical alloying in Ni–Al and Cu–Zn systems, Mater. Sci. Eng. A 214 (1996) 146–152.
[21] M.F. Giordana, M.R. Esquivel, E. Zelaya, A detailed study of phase evolution in Cu-16 at.%Al and Cu-30 at.%Al alloys under different types of mechanical alloying processes, Adv. Powder Technol. 26 (2) (2015) 470–477.
[22] M.F. Giordana, N. Muñoz-Vásquez, M. Garro-González, M.R. Esquivel, E. Zelaya, Study of the formation of Cu-24at.%Al by reactive milling, Proc Mater. Sci. 9 (2015) 262–270.
[23] M.F. Giordana, N. Muñoz-Vásquez, M.R. Esquivel, E. Zelaya, Analysis of the Cu-Al milling stages through the microstructure evolution studied by TEM and SEM, Metallogr. Microstruct. Anal. 6 (2) (2017) 139–149.
[24] D. Guzmán, O. Rivera, C. Aguilar, S. Ordoñez, C. Martínez, D. Serafini, P. Rojas, Mechanical alloying and subsequent heat treatment of Ag–Zn powders, Trans. Nonferrous Met. Soc. China 23 (2013) 2071–2078.
[25] J. Rodriguez-Carvajal, Satellite meeting on powder diffraction, in: Proc. of the Fifteenth Conference of the International Union of Crystallography, Toulouse, France, vol. 127, 1990.
[26] J. Rodriguez-Carvajal, Recent developments of the program FULLPROF, Comm. Powder Diffr. (IUCr) 26 (2001) 12–19.
[27] T. Saburi, C.M. Wayman, Crystallographic similarities in shape memory martensites, Acta Metall. 27 (1979) 979–995.
[28] A.M. Condo, F.C. Lovey, V. Torra, Interaction of twin boundaries with stacking faults in 2H martensite: A high-resolution electron microscopy study, Phil. Mag. 83 (12) (2003) 1479–1493.
[29] P.M. La Roca, L.M. Isola, C.E. Sobrero, P. Vermaut, J. Malarría, Grain size effect on the thermal-induced martensitic transformation in polycrystalline Cu-based shape memory alloys, Mater. Today: Proc. 2 (2015) S743–S746.
[30] M.T. Ochoa-Lara, H. Flores-Zúñiga, D. Rios-Jara, Study of $\gamma 2$ precipitation in Cu-Al-Be shape memory alloys, J. Mater. Sci. 41 (17) (2006) 5455–5461.
[31] A. Ibarra, J. San Juan, E.H. Bocanegra, M.L. Nó, Evolution of microstructure and thermomechanical properties during superelastic compression cycling in Cu–Al–Ni single crystals, Acta Mater. 55 (2007) 4789–4798.
[32] R. Gastien, M. Sade, F.C. Lovey, The inhibition of γ' martensite in $\beta \leftrightarrow \beta' + \gamma'$ cycling in Cu-Al-Ni single crystals, Mater. Sci. Eng. A 481–482 (2008) 518–521.

Please cite this article in press as: N.N. Sanchez Pascal et al., Thermal stability analysis of Cu-11.8 wt%Al milled samples by TEM and HT-XRD, Advanced Powder Technology (2017), http://dx.doi.org/10.1016/j.apt.2017.07.012